In-situ Examination of the Selective Etching of an Alkanethiol Monolayer Covered Au111 Surface

C. O'Dwyer

PII: S0167-577X(06)01526-6
DOI: doi: 10.1016/j.matlet.2006.12.043
Reference: MLBLUE 8158

To appear in: *Materials Letters*

Received date: 22 May 2006
Revised date: 18 December 2006
Accepted date: 19 December 2006

Please cite this article as: C. O'Dwyer, In-situ Examination of the Selective Etching of an Alkanethiol Monolayer Covered Au111 Surface, *Materials Letters* (2007), doi: 10.1016/j.matlet.2006.12.043

In-situ Examination of the Selective Etching of an Alkanethiol Monolayer Covered Au{111} Surface

C. O'Dwyer

Tyndall National Institute, University College Cork, Cork, Ireland

Abstract

An examination of the selective etching mechanism of a self-assembled 1-alkanethiol monolayer (SAM) covered Au{111} surface using in-situ AFM and molecular resolution STM is presented. The monolayer self-assembles on a smooth Au{111} surface and typically contains nanoscale non-uniformities such as pin-holes, domain boundaries and monatomic depressions. During etching in a ferri/ferrocyanide water-based etchant, selective and preferential etching occurs at SAM covered Au(111) terrace and step edges where a lower SAM packing density is observed, resulting in triangular islands being relieved. The triangular islands are commensurate with the Au(111) lattice with their long edges parallel to its $[1\bar{1}0]$ direction. Thus, SAM etching is selective and preferential attack is localized to defects and step edges at sites of high molecular density contrast.

I. INTRODUCTION

Over the past decade there has been considerable interest in self-assembled monolayers (SAMs) of alkanethiols on metal surfaces, most notably on Au(111) [1], which potentially allows one to prepare, tailor and optimize metallic surface properties for a variety of technological applications as well as for fundamental studies of surface phenomena [2, 3]. There have been some diverse observations with respect to the long-range structural order and integrity of chemisorbed SAMs on Au(111) [1]. Although a hydrophobic, well-ordered crystalline alkane film is required to prevent water-soluble oxidizing ions from penetrating to the underlying metal, inherent defectiveness in the SAM is magnified with suitable etchants.

Thus, the purpose of this Letter is to highlight the etching characteristics of SAM coverage on Au(111) surfaces and to introduce and characterize the conditions and process of the etching mechanism of unexposed SAMs and its dependence on the defect features present in the monolayer prior to etching. We also show that the etchant can selectively etch unexposed SAMs of relatively low packing density on Au over a period of time.

II. EXPERIMENTAL

Details on the substrate preparation, growth of the SAM and conditions of AFM and STM imaging can be found elsewhere [4, 5]. In-situ etching took place in an in-house-fabricated cell amenable to normal AFM operation using a water-based etching solution composed of 1 mol dm^{-3} KOH, 0.1 mol dm^{-3} $K_2S_2O_3$, 0.01 mol dm^{-3} $K_3Fe(CN)_6$ and 0.001 mol dm^{-3} $K_4Fe(CN)_6$.

Topological information acquired during AFM examination was supplemented by lateral force and phase modulation imaging respectively to determine adhesion force changes and

composition differences in the surfaces examined.

III. RESULTS AND DISCUSSION

We have been able to produce Au{111} films using a sputtering technique and it has allowed us to establish an easy preparation of atomically flat Au films. A typical example of such a surface is shown in Fig. 1a. Once the SAM has formed, we observe that its structure is prone to defect formation due to self-assembly on the Au{111} surface. It was previously reported that missing-row defects, such as those shown at **A** and **B** in the molecular resolution STM image in Fig. 1b, are attributed to rotational and translational domain boundaries within the SAM [3]. The pits observed on the surface (highlighted by arrows) are characteristic of this system [6]. Lower magnification STM studies of the surface, presented in Fig. 2a, show the presence of larger, triangular-shaped VIs within the domain-structured SAM. In Fig. 2a, several monatomic terraces of the Au lattice can be observed and VIs are present on each terrace level; they are most often observed in the vicinity of a monatomic step-edge. The constant current image is presented in height-mapped greyscale and thus, for each grey intensity (*i.e.* each terrace), the VIs are noted to be darker than the surrounding SAM. A corresponding line scan through the image crossing a VI and a monatomic step edge is show below Fig. 2b. The origin of the VIs is still not definitively clear [7], but it is established that the depth of the VIs is equivalent to the depth of a monolayer of Au(111), *i.e.* $\sim$0.24 nm.

Figure 2c shows an atomic resolution STM image of the SAM. The orientation of the SAM with respect to the substrate is determined by the weaker positional dependence of the monolayer to the Au surface, meaning that the SAM tends to minimize the strain by aligning one of its main crystalline axes along specific crystalline directions of the substrate.

The presence of a rotational boundary within the monolayer is also visible, defined by the dashed line. The alignment of the SAM is such that the unit cell short axis is parallel to the $\langle 112 \rangle$ directions of the Au lattice and the long axis is parallel to the $\langle 110 \rangle$ directions. A prominent Au step edge can also be seen in Fig. 2c. The majority of steps on Au(111) run along the $[1\bar{1}0]$ direction [8, 9]. The orientation of the sides of the SAM molecular unit cell on a step edge, as determined by STM, are $[1\bar{1}0]$ and $[11\bar{2}]$, respectively. Consequently, at a step edge, Au atoms on the upper Au terrace exist as an adlattice in the three-fold hollow sites of the lower Au terrace. This occupancy causes a mismatch in the positioning of the SAM molecules, which would ordinarily have occupied these positions, resulting in a lower density of SAM molecules in the vicinity of the boundary.

For investigation of the defect-induced selective etching mechanism, experiments were carried out in which a specific area (typically 10 μm $\times$ 10 μm) of the surface was scanned repeatedly by AFM. Figure 3 shows a series of AFM images acquired in-situ immediately after the SAM covered Au substrate was placed in the etching solution. After $\sim$85 s, a pronounced etching morphology develops with the relief of triangular shaped features. Their density is reduced by >70% after a further 85 s. Continued etching time results in almost all triangular features being removed from the surface and eventual pitting of the Au after 40 s. This is in good agreement with our previous observations [4, 5] where a 30 nm thick SAM covered Au layer becomes pitted after 5 mins and etches completely after 25-30 mins. Since each image was scanned from top to bottom in real time, it is of course obvious that the lower portion of each image shows a more pronounced etch morphology than the corresponding upper portion of the same image. The two longest adjacent edges of each etch feature are parallel to the substrate and separated by an angle of $\sim$30°. The longest sides of all features are parallel to each other and to the $\langle 110 \rangle$ lattice vectors of the

Au surface.

We also employed both phase and lateral force imaging AFM techniques to characterize the SAM/Au surface during the first 70 s of etching. Figure 4 shows a series of lateral force images of the surface acquired in-situ over this time period. Both topographical and lateral force imaging were acquired simultaneously for comparison. In this case, the alkanethiol monolayer is shown in bright gray and the Au surface is black. The pristine SAM imaged in this manner is shown in **A**. It can be observed in **B** that, after ∼14 s saturation coverage by the alkanethiol is effectively maintained. Although this is the first time-sequence image acquired, we assume that the black colored features (Au) appear due to the etching process and not due to large defects in the SAM. After 28 s, we observe an increase in black colored features (**C**) and further SAM removal occurs in the succeeding 14 s as evidenced in **D**. Considerable etching begins to occur after a further 14 s and this trend continues, as seen in **E**, resulting in considerably more SAM removal and the observation of triangular features relieved by SAM desorption, highlighted by arrows in **F**. Thus, in the first 70 s, SAM removal occurs initially slowly and proceeds with a relatively constant rate (based on AFM images **C**−**E**) and results in triangular shaped features forming in the SAM, relieving the Au surface underneath for etching.

Figures 5a and 5b show topographical and lateral force images of the surface, respectively, acquired in-situ after 170 s of etching. A careful analysis of the triangular island in Fig. 5a shows that the edges are parallel to three directions of the six-fold symmetry of the Au(111) lattice vectors with respect to the crystallographic orientation calibration outlined earlier; the longest edge is parallel to the Au(111) lattice along its $[1\bar{1}0]$ direction. As outlined earlier, a lower density of SAM packing is observed in the vicinity of terraces and monatomic step edges. Also, the etch resistance of SAM depends entirely on a well-ordered, hydrophobic

SAM to prevent etchant penetration. Since the SAM's hexagonal packing arrangement is commensurate with the (111) lattice along its ⟨112⟩ directions [3] and has its highest molecular density on Au{111} terraces, we surmize that the directionality of triangular etch features is due to the molecular density contrast of the alkanethiol monolayer.

The lateral force image in Fig. 5b was acquired simultaneously with Fig. 5a. The brightly coloured areas represent SAM molecules and the dark areas represent relieved Au surface. It is clearly observed that the triangular features are covered with SAM, however, a considerable amount of SAM still remains on the inter-island surface after 85 s (cf. Fig. 3a). This indicates that, although the etching mechanism is selective and seemingly preferential at step edges where virtually no SAM remains, low defect density areas are also susceptible to etching in short periods of time. Analysis of defect density in STM images such as that shown in Fig. 6, and subsequent comparison to etch feature density found in images similar to Fig. 4, evidences a similarity in the density of etched features and the density of defects in the SAM prior to etching. Thus, we can ascribe these observations to the presence of defects within the saturation coverage SAM. A recent observation [10] suggests that water penetration can occur to a limited extent in silane monolayers on Au{111} at edges of islands and near defects, where packing may be less than optimal.

Because alkanethiol molecules pack with the lowest defect density on {111} surfaces, their presence after extended etching times infers their chemical resistance and impermeability to water-based ions. However, in the vicinity of defects and monatomic step edges, comparatively lower SAM packing density areas become susceptible to ion penetration, resulting in a three-fold symmetrical selective etching mechanism.

Acknowledgments

The author acknowledges support through the European Community's Human Potential Programme under contract HPRN-CT-2002-00304 and from Science Foundation Ireland (SFI) under Investigator Award 02/IN.1/172.

[1] A. Ulman, Chem. Rev. 96 (1996) 1533.

[2] F. Schreiber, Prog. Surf. Sci. 65 (2000) 151.

[3] C. O'Dwyer, G. Gay, B. Viaris de Lesegno, J. Weiner, Langmuir 20 (2004) 8172.

[4] C. O'Dwyer, G. Gay, B. Viaris de Lesegno, J. Weiner, K. Ludolph, D. Albert, E. Oesterschulze, J. Appl. Phys. 97 (2005) 114309.

[5] C. O'Dwyer, G. Gay, B. Viaris de Lesegno, J. Weiner, M. Mützel, M. Haubrich, D. Meschede, K. Ludolph, D. Albert, E. Oesterschulze, J. Phys.: Conf. Series 19 (2005) 109.

[6] C. Schonenberger, J. A. M. Sondag-Huethorst, J. Jorritsma, L. G. Fokkink, Langmuir 10 (1994) 611.

[7] J. J. Benitez, D. F. Ogletree, M. Salmeron, Langmuir 19 (2003) 3276.

[8] I. Chizov, G. Scoles, A. Kahn, Langmuir 16 (2000) 4358.

[9] I. Chizov, A. Kahn, G. Scoles, J. Cryst. Growth 208 (2000) 449.

[10] I. Díez-Pérez, M. Luna, F. Teherán, D. F. Ogletree, F. Sanz, M. Salmeron, Langmuir 20 (2004) 1284.

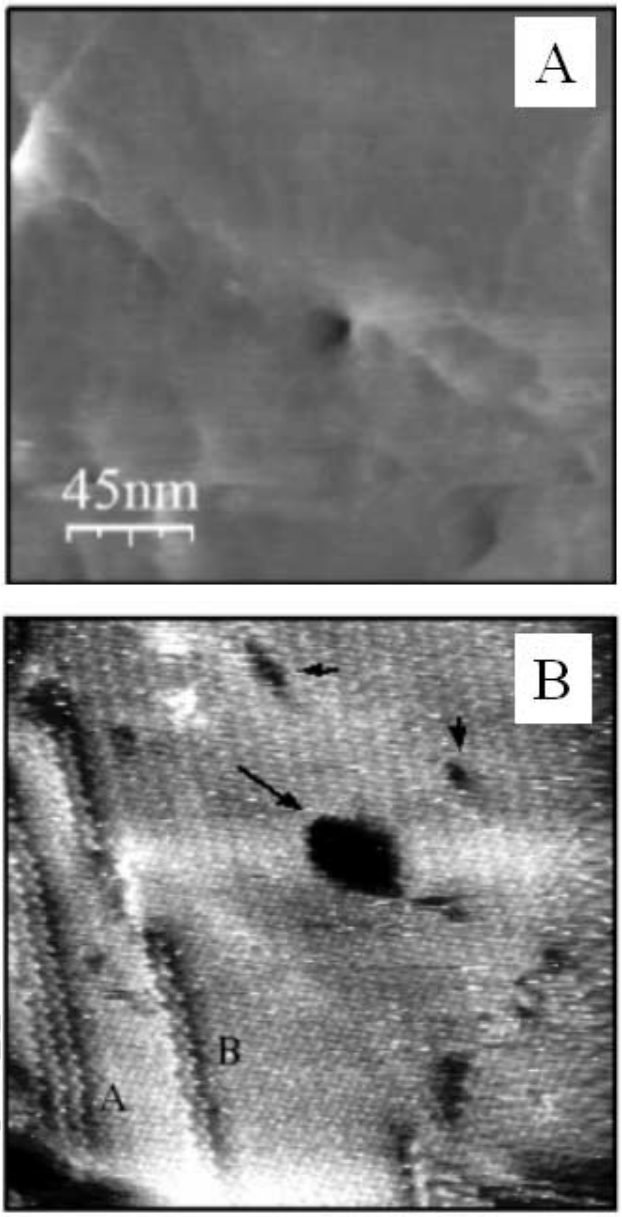

FIG. 1: (a) 250 nm × 250 nm tapping mode survey AFM image of the Au{111} surface immediately prior to immersion in the alkanethiol bath solution. (b) 25 nm × 25 nm STM image ($V = -1.54$ V, $I = 0.12$ nA) of the alkanethiol monolayer on Au{111} at saturation coverage. Evidence for monatomically deep VIs and missing-row defect domain boundaries can also be observed.

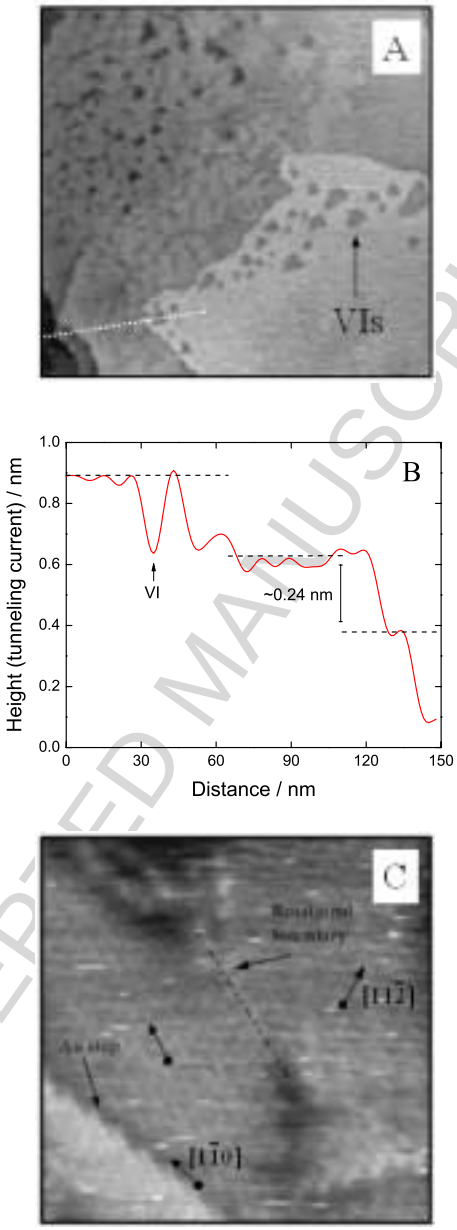

FIG. 2: (a) 200 nm × 200 nm constant current STM image (V = -1.50 V, I = 0.14 nA) of the SAM on Au{111} at saturation coverage. The image is presented in height-mapped grayscale. (b) Profile of the height corresponding to the line drawn on (a) traced from right to left in the image. The monatomic height (∼0.24 nm) of Au(111) is indicated for comparison. (c) 9 nm × 9 nm molecular resolution STM image of a rotational boundary in the SAM. The edge of the prominent Au step is indicated by the arrow and is parallel to the Au[1$\bar{1}$0] direction.

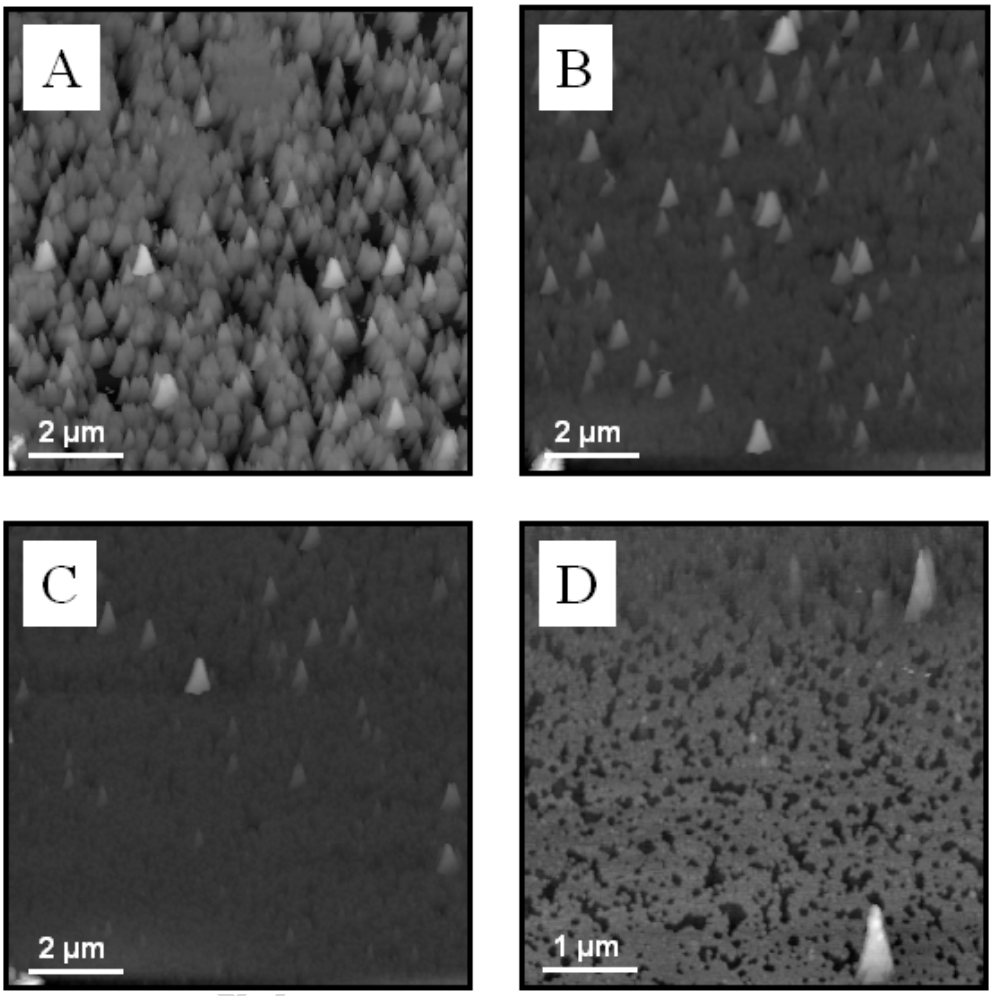

FIG. 3: AFM images of the alkanethiol covered surface acquired in-situ after immersion into the etching solution. AFM scans were conducted at a scan rate of 3 Hz, corresponding to 85 s scanning time per image. Image acquisition commenced immediately and each successive image was sampled over a period of 85 s with negligible latent time between each image. Thus, the data was acquired after intervals of (a) 85 s (b) 170 s (c) 255 s and (d) 340 s.

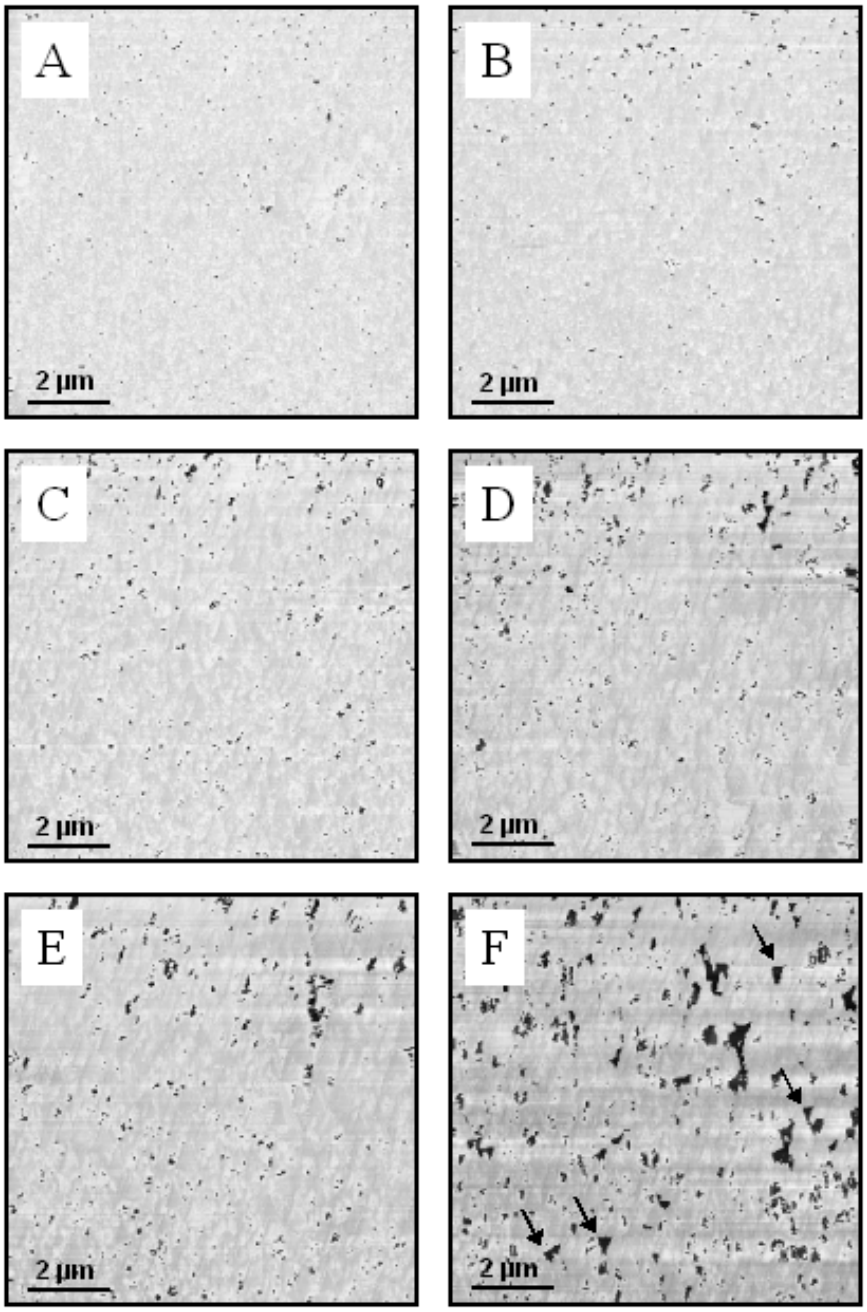

FIG. 4: AFM lateral force images of the alkanethiol covered surface acquired in-situ after immersion into the etching solution. Image acquisition commenced immediately and each successive image was sampled after intervals of (a) 0 s (b) 14 s (c) 28 s (d) 42 s (e) 56 s and (f) 70 s. The appearance of triangular features in the SAM in (f) is highlighted in certain areas by arrows.

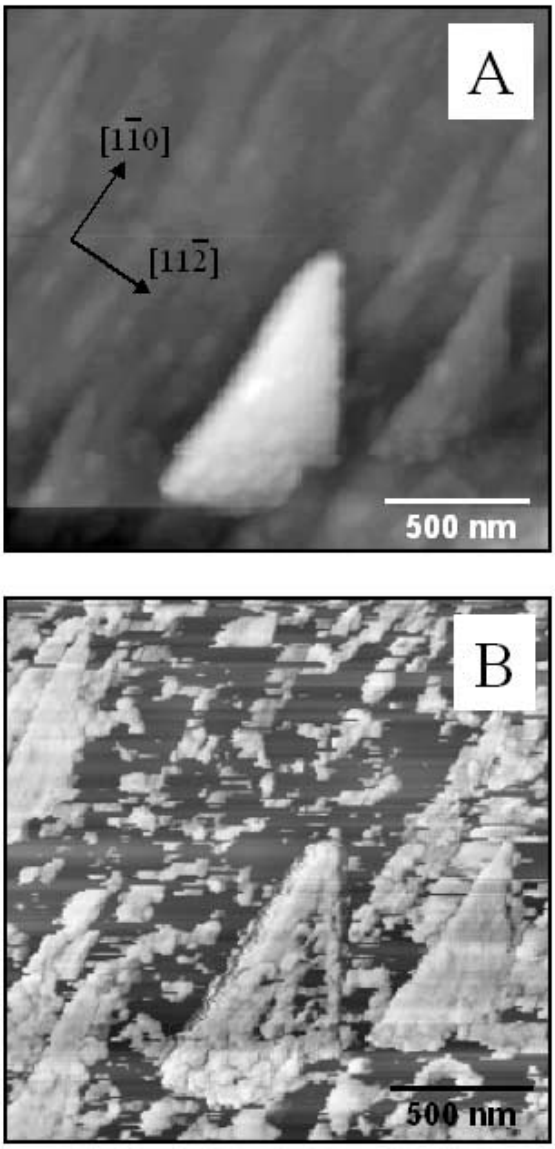

FIG. 5: (a) Topographical AFM image of the alkanethiol monolayer covered Au{111} surface acquired 170 s after immersion in the etching solution (b) corresponding phase image of the same area of surface acquired simultaneously.

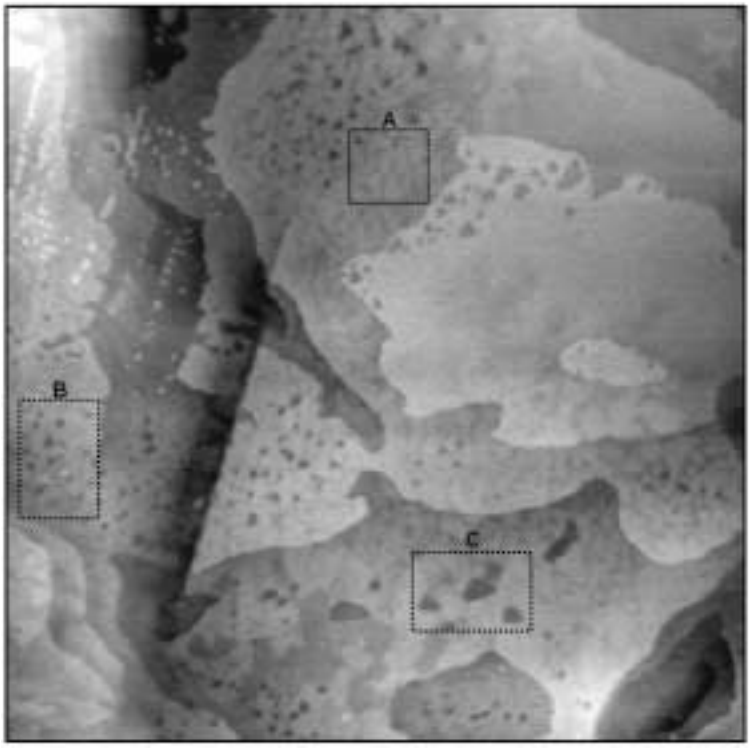

FIG. 6: 425 nm × 425 nm STM image of the 1-nonanethiol on Au{111} terraces in height-mapped greyscale, where a large number of non-uniformities such as domain boundaries (**A**), pinholes (**B**) and monatomic depressions (**C**) are observed on the Au{111} terraces.